NeuroImage: Clinical 19 (2018) 858–867

Contents lists available at ScienceDirect

NeuroImage: Clinical

journal homepage: www.elsevier.com/locate/ynicl

Autosomal dominant cerebellar ataxias: Imaging biomarkers with high effect sizes

Isaac M. Adanyeguh[a], Vincent Perlbarg[a,b], Pierre-Gilles Henry[c], Daisy Rinaldi[a], Elodie Petit[a], Romain Valabregue[a,d], Alexis Brice[a], Alexandra Durr[a,e], Fanny Mochel[a,e,f,*]

[a] INSERM U 1127, CNRS UMR 7225, Sorbonne Universités, UPMC Univ Paris 06 UMR S 1127, Institut du Cerveau et de la Moelle épinière, ICM, F-75013 Paris, France
[b] Bioinformatics and Biostatistics Core Facility, iCONICS, Institut du Ceveau et de la Moelle épinière, ICM, F-75013 Paris, France
[c] Center for Magnetic Resonance Research (CMRR), University of Minnesota, Minneapolis, MN, United States
[d] Center for NeuroImaging Research (CENIR), Institut du Cerveau et de la Moelle épinière, 75013 Paris, France
[e] AP-HP, Pitié-Salpêtrière University Hospital, Department of Genetics, Paris, France
[f] University Pierre and Marie Curie, Neurometabolic Research Group, Paris, France

ARTICLE INFO

Keywords:
Spinocerebellar ataxia
Imaging biomarkers
Apparent fiber density
Fixel analysis
Diffusion imaging.

ABSTRACT

Objective: As gene-based therapies may soon arise for patients with spinocerebellar ataxia (SCA), there is a critical need to identify biomarkers of disease progression with effect sizes greater than clinical scores, enabling trials with smaller sample sizes.

Methods: We enrolled a unique cohort of patients with SCA1 (n = 15), SCA2 (n = 12), SCA3 (n = 20) and SCA7 (n = 10) and 24 healthy controls of similar age, sex and body mass index. We collected longitudinal clinical and imaging data at baseline and follow-up (mean interval of 24 months). We performed both manual and automated volumetric analyses. Diffusion tensor imaging (DTI) and a novel tractography method, called fixel-based analysis (FBA), were assessed at follow-up. Effect sizes were calculated for clinical scores and imaging parameters.

Results: Clinical scores worsened as atrophy increased over time ($p < 0.05$). However, atrophy of cerebellum and pons showed very large effect sizes (> 1.2) compared to clinical scores (< 0.8). FBA, applied for the first time to SCA, was sensitive to microstructural cross-sectional differences that were not captured by conventional DTI metrics, especially in the less studied SCA7 group. FBA also showed larger effect sizes than DTI metrics.

Conclusion: This study showed that volumetry outperformed clinical scores to measure disease progression in SCA1, SCA2, SCA3 and SCA7. Therefore, we advocate the use of volumetric biomarkers in therapeutic trials of autosomal dominant ataxias. In addition, FBA showed larger effect size than DTI to detect cross-sectional microstructural alterations in patients relative to controls.

1. Introduction

Spinocerebellar ataxias types 1 (SCA1), 2 (SCA2), 3 (SCA3) and 7 (SCA7) are rare autosomal dominant ataxias caused by expanded CAG triplet repeats (Durr, 2010; Rüb et al., 2013). Among the dominantly inherited SCA, SCA7 presents additional non-neurological symptoms such as retinal degeneration and cardiomyopathy, commonly found in patients with mitochondrial dysfunction. Currently, the most common clinical scores for rating the disease severity are the Scale for the Assessment and Rating of Ataxia (SARA) (Schmitz-Hübsch et al., 2006) and the Composite Cerebellar Functional Severity Score (CCFS) (du Montcel et al., 2008). However, they cannot be used to evaluate pre-manifest individuals and their small effect size would require large numbers of patients in clinical trials, which is an issue due to the scarcity of SCA. As gene-based therapies are showing promise in preventing or reversing SCA pathophysiology (Keiser et al., 2015; 2016), there is a need for biomarkers with effect sizes greater than clinical scores, which can be used in trials on small sample sizes.

Abbreviations: CCFS, composite cerebellar functional severity score; CFE, connectivity-based fixel enhancement; CSD, constrained spherical deconvolution; CST, corticospinal tract; DTI, diffusion tensor imaging; FA, fractional anisotropy; FBA, fixel-based analysis; FC, fiber cross-section; FD, fiber density; FDC, fiber density and cross-section; FOD, fiber orientation distribution; FOV, Field of view; GRAPPA, generalized autocalibrating partial parallel acquisition; MPRAGE, magnetization-prepared rapid gradient-echo; MRI, magnetic resonance imaging; RD, radial diffusivity; SARA, scale for the assessment and rating of ataxia; SCA, spinocerebellar ataxias; SNR, signal-to-noise ratio; TBSS, tract-based spatial statistics; TE, echo time; TR, repetition time

* Corresponding author at: Reference Center for Neurometabolic Diseases, Department of Genetics, La Pitié-Salpêtrière University Hospital, 47 Boulevard de l'Hôpital, 75013 Paris, France.
E-mail address: fanny.mochel@upmc.fr (F. Mochel).

https://doi.org/10.1016/j.nicl.2018.06.011
Received 1 March 2018; Received in revised form 19 May 2018; Accepted 7 June 2018
Available online 14 June 2018

In Huntington disease, another trinucleotide repeat disorder, magnetic resonance imaging (MRI) techniques have been shown to be more sensitive than motor or cognitive tasks to track disease progression (Tabrizi et al., 2013). In SCA, longitudinal volumetric studies that measure the rate of atrophy and evaluate the effect size are not that numerous (Durr, 2010; Alcauter et al., 2011; D'Abreu et al., 2012; Jacobi et al., 2013; Reetz et al., 2013; Rüb et al., 2013; Mascalchi et al., 2014; Hara et al., 2016; Moriarty et al., 2016). One main study that sought to address this issue in a cohort of patients with SCA1, SCA3 and SCA6, reported on longitudinal volume loss using a 1.5 T MRI system, and the effect sizes of clinical and imaging parameters (Reetz et al., 2013). Here, we report on patients with SCA1 and SCA3, but using a 3 T MRI system, as well as in patients with SCA2 and SCA7. The primary aim of this study was to identify robust and reliable imaging biomarkers of disease progression with very large effective sizes (relative to baseline) that can be used in upcoming multicentric clinical trials in SCA. Furthermore, most studies on microstructural changes in SCA (Della Nave et al., 2004; Guerrini et al., 2004; Prakash et al., 2009; Alcauter et al., 2011; Guimarães et al., 2013; Kang et al., 2014; Hernandez-Castillo et al., 2015; Mascalchi et al., 2015; Rozenfeld et al., 2015; Yoo and Oh, 2017) reported only diffusion metrics such as fractional anisotropy (FA) that is unable to properly evaluate fiber density, particularly in brain areas with multiple fiber populations. Hence, our secondary objective was to evaluate the ability of a novel tractography technique to measure brain microstructural alterations in SCA (relative to controls) with a larger effect size than conventional methods.

2. Methods

The local ethics committee (AOM10094, CPP Ile de France VI, Ref: 105–10) approved the study. All participants were over 18 years and signed a written informed consent before they participated in the study.

2.1. Recruitment of participants

Participants were recruited as part of the BIOSCA study (NCT01470729) (Garali et al., 2017) and only those who could perform MRI and complete the follow-up imaging protocol are reported: 15 patients with SCA1, 12 patients with SCA2, 20 patients with SCA3 and 10 patients with SCA7. Twenty-four healthy individuals of similar general characteristics – median age, sex and BMI – were also enrolled (Table 1). The general characteristics of patients and controls were matched to reduce the problems of confounding factors. Subjects were excluded from the study if they were < 18 years, were unable to perform MRI, had history of significant head injury, could not complete the study protocol or unable to comprehend an informed explanation of the study protocol. Ataxia severity was evaluated with the SARA score, which ranges from 0 (no cerebellar symptoms) to 40 (most severe cerebellar symptoms) (Schmitz-Hübsch et al., 2006), and the CCFS, a composite score obtained from a nine-hole pegboard test and a click test (du Montcel et al., 2008).

2.2. Imaging protocol

MRI acquisitions were performed on a 3 T whole-body Siemens MAGNETOM Trio scanner (Siemens Medical Solutions, Erlangen, Germany) using a standard Siemens transmit body coil and 32-channel receive head coil array. The MRI system was upgraded during the study period and hence twelve datasets were acquired on a 3 T whole-body Siemens MAGNETOM Prisma scanner (Siemens Medical Solutions, Erlangen, Germany). Several phantom and volunteer scans were performed after the change to ensure that there was no difference in the data obtained on the new system. A 3D *T1*-weighted magnetization-prepared rapid gradient-echo (MPRAGE) volumetric image (T_R = 2530 ms, T_E = 3.65 ms, T_I = 900 ms, flip angle = 9°, voxel size = 1 mm isotropic, field of view (FOV) = 256 × 256 mm^2) was acquired at baseline and follow-up for volumetric analyses. Images were inspected immediately after acquisition and those with motion artifacts were reacquired immediately. Additionally, a *T2*-weighted sagittal image (T_R = 4200 ms, T_E = 80 ms, flip angle = 120°, voxel size = 0.6 × 0.5 × 5.0 mm, FOV = 240 × 240 mm^2) was acquired for each subject. The *T2*-weighted images were not included in volumetric analyses but were reviewed by a neurologist to rule out incidental brain abnormalities that could interfere with results.

Due to method development, diffusion imaging was only performed at follow-up. Diffusion data were acquired along 60 isotropic directions with echo-planar spin-echo sequence (T_R = 10,000 ms, T_E = 89 ms, voxel size = 2 mm isotropic, FOV = 220 × 220 mm^2, GRAPPA acceleration factor of 2, *b* value = 1500 s/mm^2). The directions were interleaved with five non-diffusion-weighted reference images (b0 images, *b* value = 0 s/mm^2) at every 12 directions. Another b0 image with opposite phase-encode blip was acquired. The data were corrected for motion, eddy current geometric distortions, and susceptibility-induced off-resonance field distortions.

Table 1
Demographic parameters of controls and patients with SCA.

Variable	Control	SCA1	SCA2	SCA3	SCA7
# Participants	24	15	12	20	10
Sex (M/F)	11/13	9/6	7/5	8/12	5/5
Age (yr)	50 ± 13 [26–67]	43 ± 15 [18–66]	45 ± 13 [24–59]	51 ± 12 [31–69]	48 ± 14 [23–76]
Follow-up (months)	24.3 ± 1.8 [23 − 30]	24.7 ± 2.3 [22–29]	23.6 ± 0.7 [23–25]	24.5 ± 2.1 [23–30]	23.7 ± 0.9 [23–26]
BMI (Kg/m^2)[a]	25.3 ± 3.9 [20.0–33.9]	23.6 ± 6.3 [18.2–42.8]	25.7 ± 4.6 [19.4–37.3]	23.7 ± 4.5 [15.4–38.7]	22.1 ± 1.8 [19.5–25.3]
BMI (Kg/m^2)[b]	25.3 ± 3.6 [19.7–33.6]	23.6 ± 6.7 [17.0–43.6]	26.6 ± 4.4 [21.7–38.2]	24.1 ± 4.8 [15.7–40.7]	22.7 ± 2.6 [17.7–26.1]
SARA score[a]	0.8 ± 0.8 [0.0–3.0]	10.7 ± 6.3† [0.5–23.5]	12.6 ± 6.0† [3.0–22.0]	13.0 ± 7.2† [0.0–24.5]	8.3 ± 7.4† [0.0–21.5]
SARA score[b]	0.7 ± 0.7 [0.0–2.0]	13.2 ± 7.0† [1.5–24.5]	14.4 ± 6.3† [5.0–29.0]	15.2 ± 7.5† [1.0–28.0]	9.5 ± 8.3† [0.0–23.0]
CCFS[a]	0.9 ± 0.1 [0.8–1.0]	1.0 ± 0.1† [0.9–1.3]	1.1 ± 0.1† [0.9–1.4]	1.0 ± 0.1† [0.9–1.2]	1.0 ± 0.2† [0.8–1.3]
CCFS[b]	0.8 ± 0.0 [0.8–0.9]	1.1 ± 0.2† [0.9–1.3]	1.1 ± 0.2† [0.9–1.5]	1.1 ± 0.1† [0.9–1.3]	1.0 ± 0.2† [0.8–1.5]
CAG length	–	47 ± 7 [40–62]	40 ± 3 [36–46]	69 ± 6 [50–75]	41 ± 3 [36–44]
Disease duration[a]	–	7 ± 6 [1 − 21]	10 ± 6 [2 − 20]	9 ± 5 [1–16]	9 ± 6 [2–18]
Disease duration[b]	–	9 ± 6 [3 − 23]	12 ± 6 [4–22]	11 ± 5 [3–18]	11 ± 5 [4–20]

Data are presented as mean ± standard deviation. $^{\dagger}p \leq 0.001$ and $^{\#}p \leq 0.01$ represent significant differences between SCA and controls obtained with the analysis of covariance, controlling for age, and with the step-down Bonferonni multiple correction. There was no difference in demographic parameters between the SCA.

[a] Parameters at baseline.

[b] parameters at follow-up.

2.3. Volumetric analyses

The implementation of brain volumetry markers in large trials necessitates reproducible and reliable measurement processes. This suggests the use of automated segmentation while the gold standard in SCA evaluation remains the manual segmentation. Two strategies of segmentation were thus used and compared: manual segmentation – the gold standard – performed by one expert using ITK-SNAP (Yushkevich et al., 2006), and an automated segmentation using the Freesurfer software (Fischl et al., 2002). Since manual segmentation is highly time-consuming, we chose to manually segment only the cerebellar vermis, the region mostly affected in this SCA and from which neurometabolic alterations were previously reported (Adanyeguh et al., 2015). After linearly aligning the image along the midline, the vermis lobules were delineated on the mid-sagittal slice, excluding the cerebellar tonsils (Supplementary eFig. 1). This was repeated on only four slices each to the right and left of the mid-sagittal slice due to poor contrast in subsequent slices.

To reduce the bias from inter- and intra-individual morphological variability and improve the reliability of the volume estimation, the longitudinal stream of Freesurfer version 5.3 was applied to the data (Reuter et al., 2012). The longitudinal stream is more robust and reliable compared to cross-sectional analysis as the parcellations are initialized with a within-subject template that is created using robust, inverse consistent registration (Reuter et al., 2010; 2012). We defined the volume of the cerebellum as the sum of the cerebellar cortex and cerebellar white matter parcellations. Segmentation of the brainstem to extract the pons was based on probabilistic atlas and Bayesian inference approach (Iglesias et al., 2015) implemented in Freesurfer version 6. The segmented images were visually inspected to detect segmentation errors and the need for manual editing. The segmentation process was however very good and there was no need for manual correction. All reported brain volumes were normalized to the total intracranial volume estimated from the longitudinal Freesurfer pipeline.

2.4. Rate of atrophy

The rate of atrophy of the cerebellum and the pons, two regions primarily affected in SCA (Durr, 2010; Rüb et al., 2013), was calculated as the percentage change, relative to baseline, of the cerebellar and pontine volumes estimated from automated segmentation, and normalized to the time between visits (Reetz et al., 2013).

$$Rate\ of\ atrophy = \frac{\left(\frac{followup\ value - baseline\ value}{baseline\ value}\right)}{visit\ interval\ (months)}$$

The same formula was used to determine the rate of change of clinical scores.

2.5. Diffusion tensor imaging

Diffusion data with extensive artifacts were excluded after inspection. Diffusion data were not acquired for two patients with SCA1, two patients with SCA3, three patients with SCA7 and two healthy controls. Few datasets did not meet the quality control criteria and had to be rejected for one patient with SCA1, two patients with SCA2, two patients with SCA3 and one healthy control. Data were denoised (Veraart et al., 2016) to improve the signal-to-noise ratio (SNR). Topup (Andersson et al., 2003) and eddy (Andersson and Sotiropoulos, 2016) were applied to correct eddy current, motion and susceptibility-induced off-resonance field distortions. The diffusion tensor model was fitted to generate FA and radial diffusivity (RD) maps. We did not focus on axial diffusivity maps since they do not always match the underlying fiber tract direction (O'Donnell and Westin, 2011). FA indicates fiber integrity and decreased FA usually reflects reduced fiber bundle. RD represents diffusion across the fibers and increased RD often correlates with changes in axonal diameter, demyelination or myelin injury. Tract-based spatial statistics (TBSS) with threshold-free cluster enhancement (Smith et al., 2006) was performed on FA and RD to compare the SCA groups with controls and to correlate FA with atrophy of the cerebellum and pons using a two-sample unpaired *t*-test with 5000 permutations. For each SCA group, a mask was created from regions that showed significant differences in FA and RD. The mean FA and RD values within this mask were then calculated for each patient and used for correlation analyses with clinical parameters.

2.6. Tractography - fixel based analysis

Though the DTI model is widely used, it is limited in its ability to distinguish between different fiber populations within a voxel (Alexander et al., 2002). We thus performed whole brain statistical analyses on specific fiber populations in a voxel known as fixel (Raffelt et al., 2015; 2017). The processing steps have previously been fully detailed (Raffelt et al., 2015; 2017) and were performed using the MRtrix software version 0.3.15. The constrained spherical deconvolution (CSD) approach that accounts for non-white matter tissue composition (Dhollander et al., 2016) was used to estimate the fiber orientation distribution (FOD) from the averaged response function of all subjects. Twenty controls and twenty patients were used to generate a population template to which all subjects' FOD was registered. The FODs in the template space were segmented to estimate fiber density (FD), fiber cross-section (FC) and a combination of both, FDC (Raffelt et al., 2017). FD relates to the volume of the intra-axonal compartment for a fixel, while FC refers to the volume perpendicular to the fiber bundle. The connectivity-based fixel enhancement (CFE) (Raffelt et al., 2015) was used to perform statistical analyses between SCA groups and controls on FD, FC and FDC with 5000 permutations and family-wise error corrected significance at $p < 0.05$. CFE is a threshold-free cluster enhancement approach that first uses the generated whole-brain template tractogram to identify fixels that are structurally connected and then applies a local smoothing to the tract-specific fixels before statistical maps are generated (Raffelt et al., 2015). For each SCA group, a mask was created from regions that showed significant differences in FDC. The mean fixel values within this mask were then calculated for each patient and used for correlation analyses with clinical parameters and the rate of atrophy.

2.7. Statistical analyses

2.7.1. Longitudinal analysis

The differences in clinical parameters and volumetric measures between baseline and follow-up within each group were evaluated with linear mixed modeling accounting for repeated measures and using age as a covariate centered on the group mean. Significant results were corrected for multiple testing with Bonferroni correction.

The rate of motor decline (assessed by the SARA score and the CCFS) and the rate of atrophy were evaluated using analysis of covariance whilst controlling for age, and when significant, step-down Bonferonni correction was performed to correct for multiple comparison between each SCA group and the control group.

Finally, the effect sizes over time for clinical scores, manual segmentation and automated segmentation by Freesurfer were calculated as the mean change to the standard deviation of the change (Reetz et al., 2013).

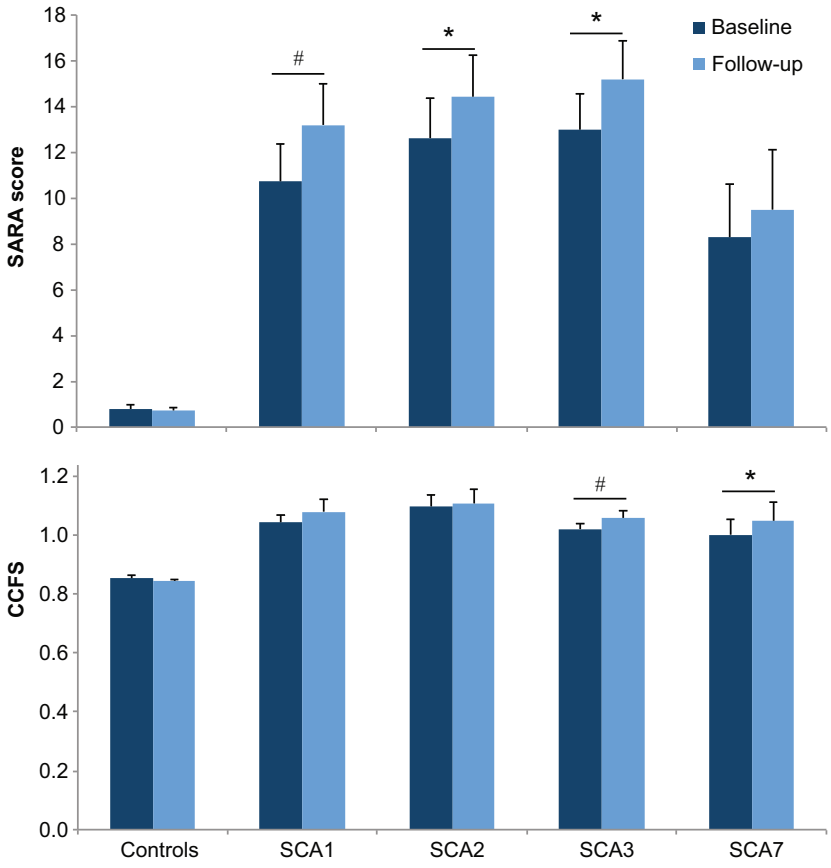

Fig. 1. Change in clinical scores between baseline and follow-up. All SCA groups showed increased SARA scores that reached significance in SCA1, SCA2 and SCA3. CCFS was also significantly increased in patients with SCA3 and SCA7. Error bars represent standard error of mean (SEM). * $p < 0.05$ and $^{\#}p \leq 0.01$ represent significant differences adjusted for age and corrected with Bonferroni correction.

$$Effect\ size = \frac{\sum\left(\frac{\left(\frac{followup\ value - baseline\ value}{baseline\ value}\right)}{visit\ interval\ (months)}\right) \div N}{SD\,(change\ in\ value)}$$

Where SD represents standard deviation and N represents number of subjects.

The scale for the effect size was set at 0.2, 0.5, 0.8, 1.2 and 2.0 as small, medium, large, very large and huge changes, respectively (Cohen, 1988; Sawilowsky, 2009).

2.7.2. Cross-sectional analysis

Cross-sectional analyses were conducted on data acquired during the second visit (follow-up), including diffusion weighted imaging not acquired at baseline. Between group differences of clinical and imaging parameters were evaluated using analysis of covariance whilst controlling for age, and when significant, step-down Bonferonni correction was performed to correct for multiple comparison. For each SCA group also, Pearson correlation was performed between diffusion imaging parameters and conventional markers (clinical scores and volumes) with the step-down Bonferroni multiple correction approach; p values < 0.05 were considered significant. Finally, the effect sizes of FA and FDC in SCA groups compared to controls were assessed by the Cohen's d (Cohen, 1988).

3. Results

3.1. Clinical scores

There was no significant difference in the SARA scores and CCFS across the SCA groups, either at baseline or at follow-up. Patients with SCA showed motor decline with increased SARA scores (patients with SCA1, SCA2 and SCA3) and/or CCFS (patients with SCA3 and SCA7) after a mean interval of 24 months (Table 1 and Fig. 1).

3.2. Volumetric analyses

Manual segmentation was not sensitive to detect longitudinal changes in volume across SCA groups except in SCA3 (Fig. 2A). Conversely, automated segmentation showed reduced volumes of the cerebellum and pons ($p < 0.05$) in all SCA groups between baseline and follow-up (Fig. 2B, C).

The rate of motor decline and atrophy between patients and controls were compared using age as a covariate. The rate of change in SARA score was not different from controls in any of the SCA groups (Fig. 3A), but the rate at which CCFS changed over time was significantly different from controls in SCA3 and SCA7 ($p < 0.05$) (Fig. 3B). Using the values obtained from the longitudinal pipeline of Freesurfer, patients with SCA showed a faster rate of atrophy in both the cerebellum and the pons compared to controls ($p < 0.05$), with the exception of the cerebellum for patients with SCA7 (Fig. 3C, D). In SCA1, CCFS correlated with the atrophy rate of the cerebellum ($r = -0.721$, $p = 0.005$) and pons ($r = -0.766$, $p = 0.004$). Furthermore, atrophy rate of the cerebellum correlated with the rate of change in SARA scores ($r = -0.811$, $p = 0.001$) and the atrophy rate of the pons correlated with the rate of change of CCFS ($r = -0.816$, $p = 0.001$). We also observed significant volume differences between patients with SCA and controls for other brain regions such as the pallidum, medulla and midbrain at baseline and follow-up (Supplementary eFig. 2).

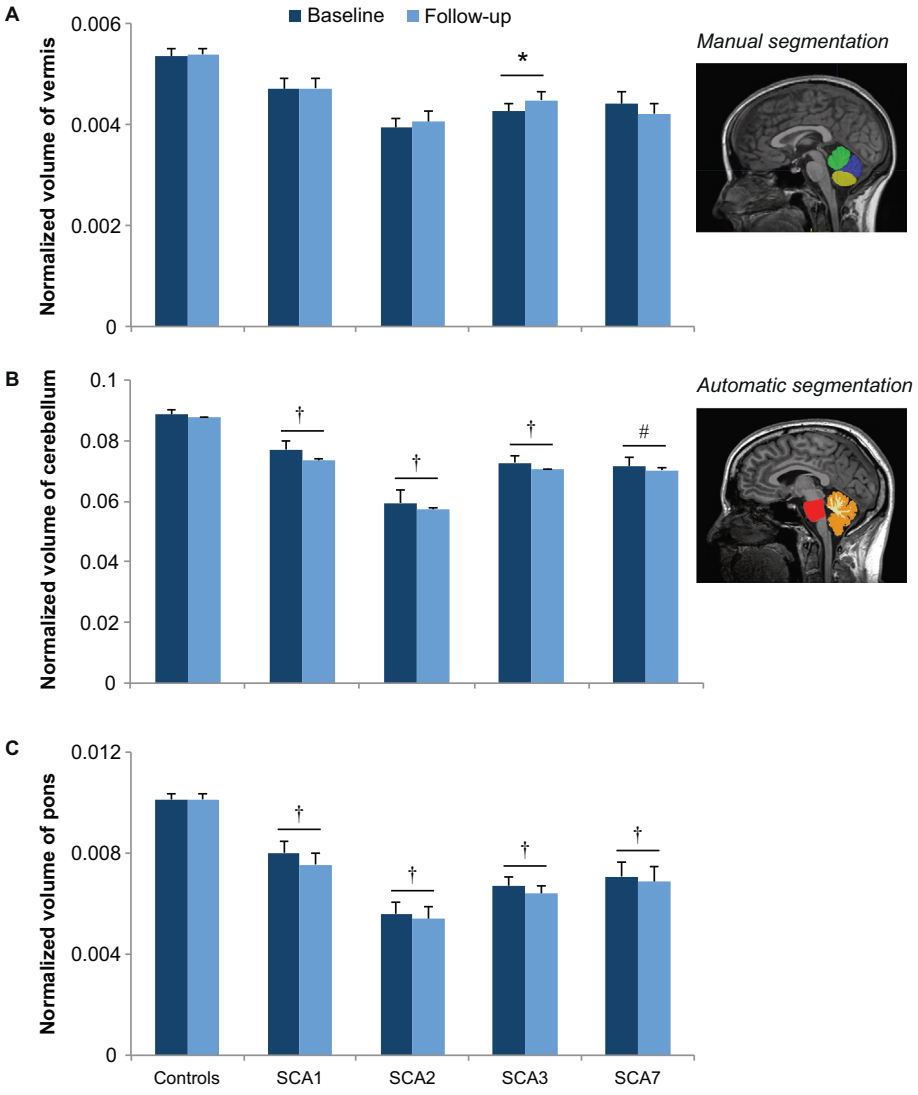

Fig. 2. Change in regional volume after 24 months. Manual segmentation of the vermis showed a significant change in volume in SCA3 only (A). Instead, Freesurfer segmentation showed a decrease in the volume of the cerebellum (B) and pons (C) in patients with SCA over 24 months. Error bars represent standard error of mean. * $p < 0.05$, $^{\#}p \leq 0.01$, and $^{\dagger}p \leq 0.001$ represent significant differences adjusted for age and corrected with Bonferroni correction.

3.3. Diffusion tensor imaging

All SCA groups displayed decreased FA compared to controls, except for patients with SCA7 (Fig. 4A). Additionally, RD was increased across all SCA groups compared to controls ($p < 0.05$) (Fig. 4B). Most of the changes in diffusion metrics were localized to the cerebellar and cerebral peduncles, as well as the pontine crossing tracts. However, the corticospinal tract (CST), corona radiata and internal capsule were also affected in patients with SCA1 and SCA2. Furthermore, the corpus callosum was altered in patients with SCA2. SARA scores correlated with FA in SCA1 ($r = -0.875$, $p = 0.002$) and SCA2 ($r = -0.807$, $p = 0.019$), and with RD in SCA1 ($r = 0.821$, $p = 0.006$), SCA2 ($r = 0.855$, $p = 0.008$) and SCA3 ($r = 0.686$, $p = 0.013$). CCFS correlated with FA in SCA1 ($r = -0.832$, $p = 0.006$), SCA2 ($r = -0.809$, $p = 0.023$) and SCA3 ($r = -0.653$, $p = 0.024$), and with RD in SCA1 ($r = 0.750$, $p < 0.001$) and SCA2 ($r = 0.780$, $p = 0.023$).

3.4. Fixel based analysis

The preprocessing steps yielded improved SNR and contrast in the datasets (Supplementary eFig. 3). A visual inspection of the FODs already showed differences between controls and patients with SCA, controls having more fiber orientations in the CST than SCA patients (Supplementary eFig. 4). Using the template fixel mask and template tractogram followed by connectivity-based fixel enhancement statistics (Fig. 5A), we found significantly decreased FD, FC and FDC in the CST of all SCA patients compared to controls ($p < 0.05$) (Fig. 5B). A significant decrease in FD was also observed in the corpus callosum of patients with SCA7 ($p < 0.05$) (Fig. 5B). FDC correlated with SARA scores in SCA1 ($r = -0.92$, $p < 0.001$) and SCA3 ($r = -0.752$, $p = 0.004$) and with CCFS in SCA1 ($r = -0.828$, $p = 0.005$), SCA2 ($r = -0.795$, $p = 0.024$) and SCA3 ($r = -0.672$, $p = 0.022$).

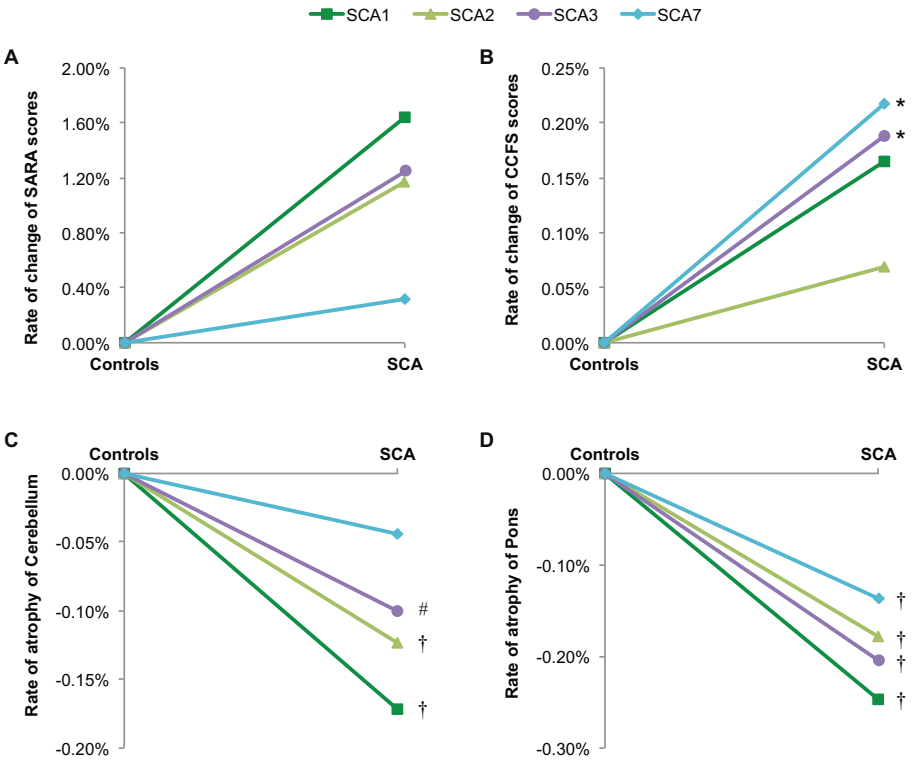

Fig. 3. Rate of motor decline and atrophy of the cerebellum and pons in patients with SCA compared to controls using age as a covariate. The change over time in SARA score was not significant (A) but the change over time of CCFS was significant in patients with SCA3 and SCA7 (B). A faster rate of atrophy was observed in the cerebellum (C) and the pons (D) of patients with SCA compared to controls, with the exception of SCA7 for the cerebellum. * $p < 0.05$, $^{\#}p \leq 0.01$, $^{\dagger}p \leq 0.001$ represent significant differences adjusted for age and corrected with step-down Bonferroni correction.

3.5. Effect sizes

Clinical scores and brain volumes were assessed at baseline and follow-up so that longitudinal effect sizes could be calculated in patients with SCA relative to baseline, using the method proposed by (Reetz et al., 2013). Clinical scores showed small effect sizes (< 0.8) whilst brain volume segmentation with Freesurfer showed very large effect sizes (> 1.2) (Table 2). Manual segmentation also showed small effect sizes (< 0.5).

Effect sizes of longitudinal data between baseline and follow-up could not be calculated for DTI and FBA metrics since diffusion data were acquired at one time point only. However, we used the Cohen's *d* (Cohen, 1988) to evaluate the effect sizes of FA and FDC of patients with SCA in reference to controls. FA and FDC showed very large effect sizes (> 1.2), the effect size of FDC being on an average 1.2 times higher than FA (Supplementary eTable).

4. Discussion

This study compared clinical scores and imaging parameters in terms of sensitivity to change in a unique cohort of patients with SCA1, SCA2, SCA3 and SCA7. Several volumetric and diffusion metrics correlated with SARA scores and CCFS in patients with SCA. Our main finding, though, was that imaging parameters showed higher longitudinal effect sizes than clinical scores in all SCA groups, making them strong candidates for use in upcoming clinical trials in SCA. In addition, we used a new, recently developed approach – fixel-based analysis (FBA) – to probe white matter fiber alterations in SCA. FBA allows the analysis of individual fibers in each voxel making it more sensitive and robust compared to FA, the conventional DTI metric. We showed that FA may not be the most accurate or sensitive metric for use in clinical trials as it detected no microstructural change in SCA7. Instead, using FBA, we identified white matter fiber changes in all SCA, including SCA7 despite the small sample size.

Volumetric studies performed in SCA have reported smaller brain regions compared to controls, including the cerebellum, brainstem and cerebellar peduncles (Durr, 2010; Jacobi et al., 2013; Rüb et al., 2013). However, the rate of longitudinal volumetric changes, i.e. the relevant outcome measure for clinical trials, has only been extensively reported by (Reetz et al., 2013) in SCA1, SCA3 and SCA6, but not SCA2 and SCA7. In patients with SCA1 and SCA3, Reetz et al. also reported large effect sizes for the SARA scores (> 1.2) and the pons atrophy (> 0.8) but small effect sizes (< 0.8) for the cerebellum (Reetz et al., 2013). Our study confirms the volumetric results of Reetz et al., but in contrast, shows small effect sizes for clinical scores (≤0.8) and large effect size (> 1.2) for the cerebellum of our SCA cohorts. The higher effect size in the cerebellum compared to Reetz et al. could likely be due in part to the higher SNR at 3 Tesla. In addition, some of the patients in our SCA cohort were at a very early stage of their disease and should have only limited cerebellar atrophy. Our findings however suggest atrophy of both the pons and cerebellum, with their large effect sizes, can be used as markers in clinical trials even in patients at a very early stage of the disease. Nonetheless, our findings need to be confirmed in an independent cohort using the same methodologies and high spatial resolution, especially in patients with SCA7 since we had a small sample size.

In patients with SCA2, even though the degree of atrophy was greater, the rate of atrophy of the cerebellum and pons was comparable or slower than in patients with SCA1 and SCA3. This could indicate increased atrophy at the early stages of the disease in SCA2, which slows as the disease progresses. In patients with SCA7, the discrepancy between the rate of clinical progression and brain atrophy was especially striking. In addition to the small sample size, this may be, in part, explained by their relative early symptomatic stage. Nonetheless, SCA7 is a severe disease, as outlined by the common occurrence of additional non-neurological symptoms (retina, heart), so that a fast rate of brain

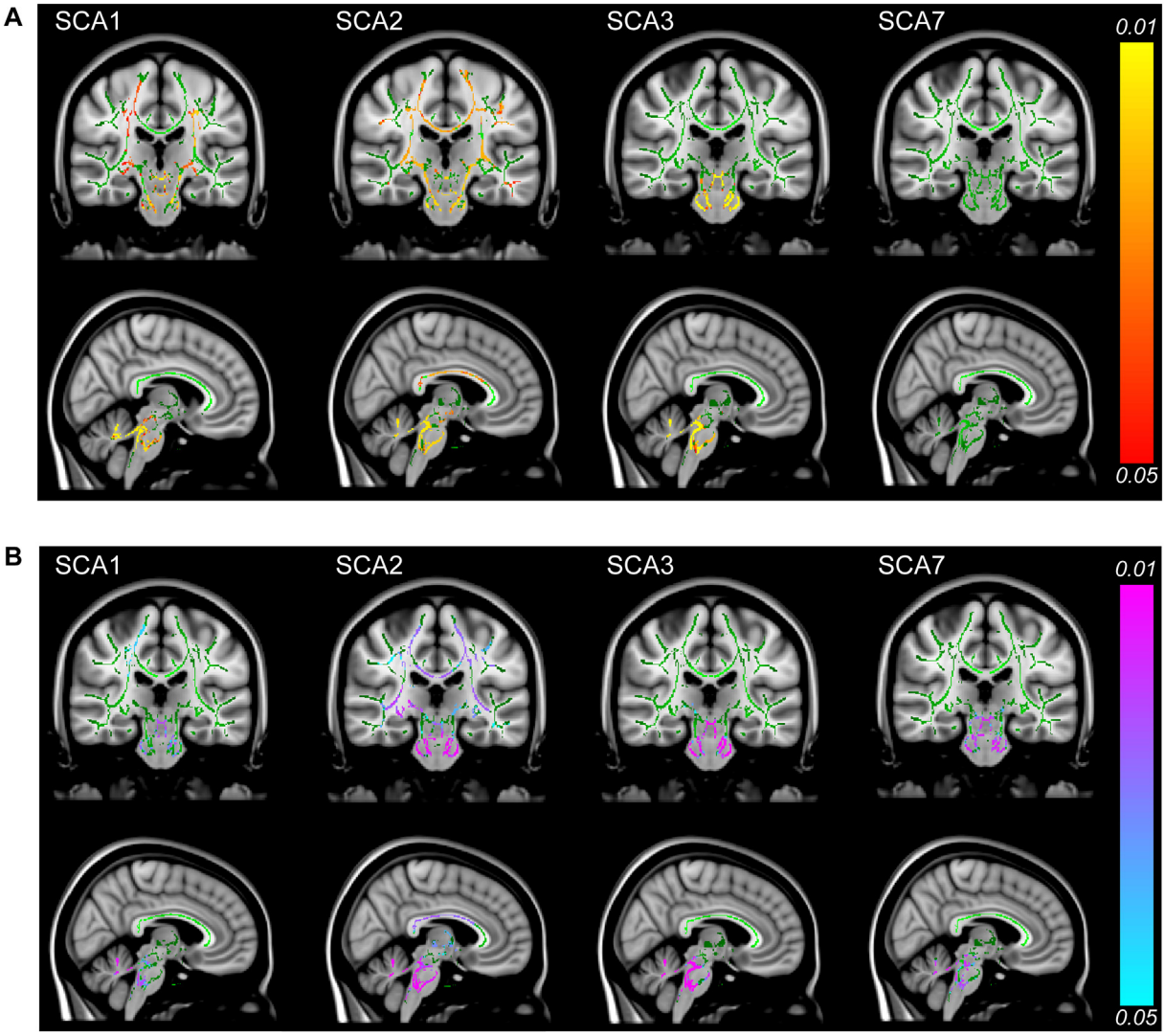

Fig. 4. Tract-based statistical analysis of FA and RD in SCA and controls. Red-yellow highlights show areas of decreased FA in SCA ($p < 0.05$) (A). Blue-pink regions show areas of increased RD in SCA ($p < 0.05$) (B).

atrophy is expected. Overall, the fact that greater atrophy was observed in patients with SCA using automated segmentation of the cerebellum compared to manual segmentation of the vermis suggests that, though the vermis is very important in SCA pathophysiology, the atrophy is not only limited to this region and the entire cerebellum should be taking into account in volumetric analysis.

Using diffusion tensor metrics, we observed decreased FA across several tracts, except in SCA7, and this was associated with increased RD in all SCA groups. Decreased FA in the corpus callosum of patients with SCA2 is in agreement with previous studies (Hernandez-Castillo et al., 2015; Mascalchi et al., 2015). In contrast to (Kang et al., 2014), we did not find any change in FA and RD in the corpus callosum, internal capsule and corona radiata in patients with SCA3. Nonetheless, because FA cannot differentiate between different fiber populations in a voxel (Alexander et al., 2002), higher-order models are needed. To resolve the limitations of FA, Rozenfeld et al. performed fiber tracking using the deterministic approach that assumes that fibers have a single orientation within each voxel and requires prior knowledge of fiber orientation (Rozenfeld et al., 2015). However, one cannot be certain of fiber orientation as each voxel contains several populations of axons that may be oriented in different directions. The deterministic approach is therefore less robust and less sensitive as compared to the probabilistic approach (Schlaier et al., 2017), which overcomes the problem of uncertainty in fiber orientation and accounts for multiple fibers in each voxel. (Kang et al., 2014) and (Prakash et al., 2009) did use the probabilistic approach but with algorithms that have more fiber orientation error rate and low fiber detection rate as compared to the non-negativity CSD approach (Wilkins et al., 2015). This is why we chose to implement a novel fiber tract specific analysis, i.e. FBA, on our SCA cohort. FBA has been successfully applied in traumatic brain injury (Wright et al., 2017), motor neuron disease (Raffelt et al., 2015; 2017) and focal epilepsy (Vaughan et al., 2017). In our study, FBA revealed decreased FD in the pontine crossing, CST, cerebral peduncle, internal capsule and corona radiata in patients with SCA1, SCA2 and SCA3. In patients with SCA7, contrary to the results obtained with FA, FD was decreased in the corpus callosum and cerebral peduncles. Together with decreased FC in these regions, decreased FD suggested a reduced number of axons in patients with SCA. Hence, longitudinal FBA data in

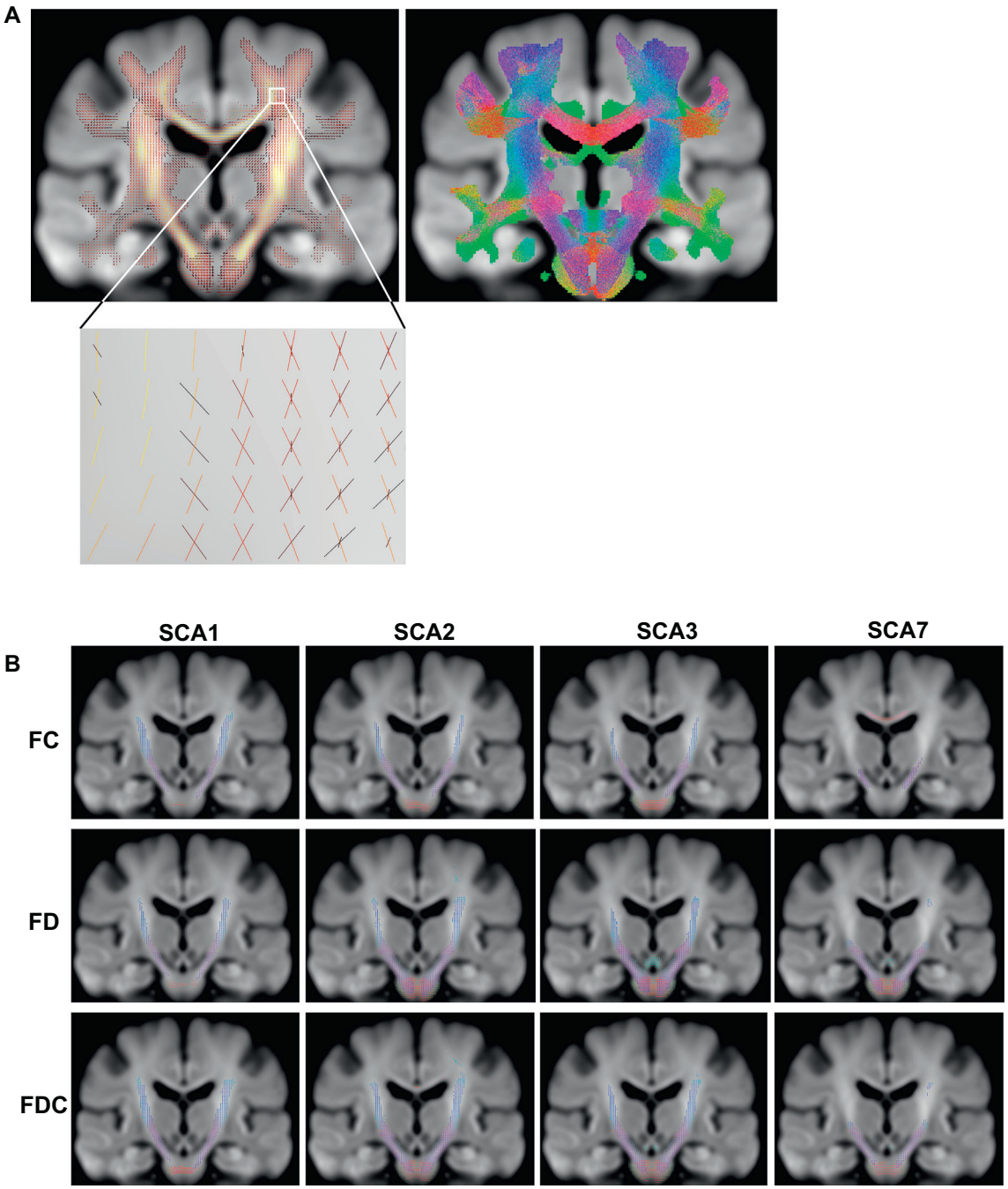

Fig. 5. Connectivity-based fixel enhancement on FD, FC and FDC. The fixel mask and tractogram used for the statistics (A). FD, FC and FDC are significantly reduced in the CST of SCA ($p < 0.05$ with family-wise error correction) (B). Fiber colours are directional: blue = superior-inferior direction; red = left-right direction; green = anterior-posterior direction.

patients with SCA would be very valuable.

In conclusion, using robust longitudinal volumetry methods that limit user interference and reduce intra- and inter-subject variability, we confirmed imaging biomarkers with large effect sizes in SCA that are promising for therapeutic trials. Though we could not calculate effect sizes on longitudinal DTI and FBA metrics, the current observations indicate that longitudinal effect sizes of FBA metrics will be greater than those of DTI metrics, highlighting their usefulness in clinical trials. Since a single biomarker is likely to fail due to the complexity of the neurodegenerative cascades leading to the onset and progression of SCA, a multimodal biomarkers approach that aims at the integration and visualization of multivariate datasets, could also be applied as we recently showed in our SCA cohort at baseline (Garali et al., 2017). In addition, although significant, the longitudinal volumetric changes reported here were relatively small. A multimodal approach may enhance sensitivity to change, especially when structural changes would not be detectable over short follow-up intervals (D'Abreu et al., 2012). Furthermore, these sensitive and robust microstructural methods hold promise for the assessment of patients with other causes of cerebellar ataxia and/or spastic paraplegia.

Table 2
Effect size of clinical scores and brain imaging parameters of controls and patients with SCA.

	Clinical scores		Brain volumetry		
	SARA	CCFS	Cerebellum (fs)	Pons (fs)	Vermis (mn)
SCA1	0.83	0.39	−1.71	−1.83	0.15
SCA2	0.77	0.17	−2.16	−1.60	0.17
SCA3	0.79	0.72	−1.47	−2.35	0.28
SCA7	0.05	0.83	−1.31	−2.06	−0.02
Control	−0.10	−0.18	−0.35	−0.07	0.03

fs: Automated longitudinal Freesurfer segmentation of cerebellum and pons; mn: manual segmentation of the vermis. The following key represents the effect size: 0.2: small, 0.5: medium, 0.8: large, 1.2: very large, 2.0: huge changes (Cohen, 1988; Sawilowsky, 2009).

Acknowledgements

We are very grateful to the patients and volunteers who participated in this study. We will also like to thank the Centre d'Investigation Clinique Pitié Neurosciences, CIC-1422 and Melanie Didier from the Center for NeuroImaging Research (CENIR) for their assistance with patients.

Conflict of interest

None reported.

Study funding

This study was sponsored by the Assistance-Publique des Hôpitaux de Paris and supported by a grant from the French Ministry of Health – “Programme Hospitalier de Recherche Clinique” [PHRC BIOSCA - ID RCB: 2010-A01324-35, AOM10094, NCT01470729] and the program “Investissements d'avenir” [ANR-10-IAIHU-06]. The Center for Magnetic Resonance Research is funded by the National Institute of Biomedical Imaging and Bioengineering (NIBIB) [P41 EB015894] and the Institutional Center Cores for Advanced Neuroimaging award [P30 NS076408].

Author contributions

Dr. Adanyeguh was involved in acquisition of data, analysis and interpretation of data, statistical analysis of data and drafting/revising the manuscript.
Dr. Perlbarg was involved in analysis and interpretation of data, statistical analysis of data and drafting/revising the manuscript.
Dr. Henry was involved in study concept and design, analysis and interpretation of data and drafting/revising the manuscript.
Dr. Rinaldi was involved in study supervision and coordination and drafting/revising the manuscript.
Ms. Petit was involved in study supervision and coordination and drafting/revising the manuscript.
Dr. Valebregue was involved in acquisition of data and drafting/revising the manuscript.
Prof Brice was involved in study concept and design and drafting/revising the manuscript.
Prof Durr was involved in the study concept and design, patient recruitment, analysis and interpretation of data and drafting/revising the manuscript.
Dr. Mochel was involved in the study concept and design, study supervision and coordination, analysis and interpretation of data, statistical analysis and drafting/revising the manuscript.

Full financial disclosure

No disclosure: Adanyeguh, Perlbarg, Rinaldi, Petit, Valabregue.
Dr. Henry received research support by grants from NIH (P41 EB015894, P30 NS076408), Bob Allison Ataxia Research Center at the University of Minnesota and Friedreich's Ataxia Research Alliance.
Prof Brice has honoraria from the Wolfson Foundation for reviewing the scientific project and from Lundbeck for giving a talk, and received research support by grants from the French Agency for Research and European Union.
Prof Durr received research support by grants from UCL/High Q Foundation and the French Agency for Research, Adverum and Pfizer Inc.
Dr. Mochel received research support by grants from INSERM, the French Agency for Research, Carnot Institutes, ASL Foundation, Ultragenyx Pharmaceutical and Ipsen.

Appendix A. Supplementary data

Supplementary data to this article can be found online at https://doi.org/10.1016/j.nicl.2018.06.011.

References

Adanyeguh, I.M., Henry, P.G., Nguyen, T.M., Rinaldi, D., Jauffret, C., Valabregue, R., Emir, U.E., Deelchand, D.K., Brice, A., Eberly, L.E., Oz, G., Durr, A., Mochel, F., 2015. In vivo Neurometabolic profiling in patients with spinocerebellar Ataxia types 1, 2, 3, and 7. Mov. Disord. 30 (5), 662–670.
Alcauter, S., Barrios, F.A., Díaz, R., Fernández-Ruiz, J., 2011. Gray and white matter alterations in spinocerebellar ataxia type 7: an in vivo DTI and VBM study. NeuroImage 55 (1), 1–7.
Alexander, D.C., Barker, G.J., Arridge, S.R., 2002. Detection and modeling of non-Gaussian apparent diffusion coefficient profiles in human brain data. Magn. Reson. Med. 48 (2), 331–340.
Andersson, J.L.R., Sotiropoulos, S.N., 2016. An integrated approach to correction for off-resonance effects and subject movement in diffusion MR imaging. NeuroImage 125, 1063–1078.
Andersson, J.L.R., Skare, S., Ashburner, J., 2003. How to correct susceptibility distortions in spin-echo echo-planar images: application to diffusion tensor imaging. NeuroImage 20 (2), 870–888.
Cohen, J., 1988. Statistical Power Analysis for the Behavioral Sciences, 2nd ed. Lawrence Erlbaum Associates, USA.
D'Abreu, A., Franca Jr., M.C., Yasuda, C.L., Campos, B.A., Lopes-Cendes, I., Cendes, F., 2012. Neocortical atrophy in Machado-Joseph disease: a longitudinal neuroimaging study. J. Neuroimaging 22 (3), 285–291.
Della Nave, R., Foresti, S., Tessa, C., Moretti, M., Ginestroni, A., Gavazzi, C., Guerrini, L., Salvi, F., Piacentini, S., Mascalchi, M., 2004. ADC mapping of neurodegeneration in the brainstem and cerebellum of patients with progressive ataxias. NeuroImage 22 (2), 698–705.
Dhollander, T., Raffelt, D., Connelly, A., 2016. Unsupervised 3-tissue response function estimation from single-shell or multi-shell diffusion MR data without a co-registered T1 image. ISMRM Work. Breaking Barriers Diff. MRI 5.
du Montcel, S.T., Charles, P., Ribai, P., Goizet, C., Le Bayon, A., Labauge, P., Guyant-Marechal, L., Forlani, S., Jauffret, C., Vandenberghe, N., N'Guyen, K., Le Ber, I., Devos, D., Vincitorio, C.M., Manto, M.U., Tison, F., Hannequin, D., Ruberg, M., Brice, A., Durr, A., 2008. Composite cerebellar functional severity score: validation of a quantitative score of cerebellar impairment. Brain 131 (Pt 5), 1352–1361.
Durr, A., 2010. Autosomal dominant cerebellar ataxias: polyglutamine expansions and beyond. Lancet Neurol. 9 (9), 885–894.
Fischl, B., Salat, D.H., Busa, E., Albert, M., Dieterich, M., Haselgrove, C., van der Kouwe, A., Killiany, R., Kennedy, D., Klaveness, S., Montillo, A., Makris, N., Rosen, B., Dale, A.M., 2002. Whole brain segmentation: automated labeling of neuroanatomical structures in the human brain. Neuron 33 (3), 341–355.
Garali, I., Adanyeguh, I.M., Ichou, F., Perlbarg, V., Seyer, A., Colsch, B., Mozer, I., Guillemot, V., Durr, A., Mochel, F., Tenenhaus, A., 2017. A strategy for multimodal data integration: application to biomarkers identification in spinocerebellar ataxia. Brief Bionform. http://dx.doi.org/10.1093/bib/bbx060.
Guerrini, L., Lolli, F., Ginestroni, A., Belli, G., Della Nave, R., Tessa, C., Foresti, S., Cosottini, M., Piacentini, S., Salvi, F., Plasmati, R., De Grandis, D., Siciliano, G., Filla, A., Mascalchi, M., 2004. Brainstem neurodegeneration correlates with clinical dysfunction in SCA1 but not in SCA2. A quantitative volumetric, diffusion and proton spectroscopy MR study. Brain 127 (Pt 8), 1785–1795.
Guimarães, R.P., D'Abreu, A., Yasuda, C.L., França, M.C.J., Silva, B.H., Cappabianco, F.A., Bergo, F.P., Lopes-Cendes, I.T., Cendes, F., 2013. A multimodal evaluation of microstructural white matter damage in spinocerebellar ataxia type 3. Mov. Disord. 28 (8), 1125–1132.
Hara, D., Maki, F., Tanaka, S., Sasaki, R., Hasegawa, Y., 2016. MRI-based cerebellar

volume measurements correlate with the International Cooperative Ataxia Rating Scale score in patients with spinocerebellar degeneration or multiple system atrophy. Cerebellum Ataxias 3, 14.
Hernandez-Castillo, C.R., Galvez, V., Mercadillo, R., Diaz, R., Campos-Romo, A., Fernandez-Ruiz, J., 2015. Extensive white matter alterations and its correlations with ataxia severity in SCA 2 patients. PLoS ONE 10 (8), e0135449.
Iglesias, J.E., van Leemput, K., Bhatt, P.C.C., Dutt, S., Schuff, N., Truran-Sacrey, D., Boxer, A., Fischl, B., 2015. Alzheimer's disease neuroimaging initiative. Bayesian segmentation of brainstem structures in MRI. NeuroImage 113, 184–195.
Jacobi, H., Reetz, K., du Montcel, S.T., Bauer, P., Mariotti, C., Nanetti, L., Rakowicz, M., Sulek, A., Durr, A., Charles, P., Filla, A., Antenora, A., Schols, L., Schicks, J., Infante, J., Kang, J.S., Timmann, D., Di Fabio, R., Masciullo, M., Baliko, L., Melegh, B., Boesch, S., Burk, K., Peltz, A., Schulz, J.B., Dufaure-Gare, I., Klockgether, T., 2013. Biological and clinical characteristics of individuals at risk for spinocerebellar ataxia types 1, 2, 3, and 6 in the longitudinal RISCA study: analysis of baseline data. Lancet Neurol. 12 (7), 650–658.
Kang, J.S., Klein, J.C., Baudrexel, S., Deichmann, R., Nolte, D., Hilker, R., 2014. White matter damage is related to ataxia severity in SCA3. J. Neurol. 261 (2), 291–299.
Keiser, M.S., Kordower, J.H., Gonzalez-Alegre, P., Davidson, B.L., 2015. Broad distribution of ataxin 1 silencing in rhesus cerebella for spinocerebellar ataxia type 1 therapy. Brain 138 (Pt 12), 3555–3566.
Keiser, M.S., Monteys, A.M., Corbau, R., Gonzalez-Alegre, P., Davidson, B.L., 2016. RNAi prevents and reverses phenotypes induced by mutant human ataxin-1. Ann. Neurol. 80 (5), 754–765.
Mascalchi, M., Diciotti, S., Giannelli, M., Ginestroni, A., Soricelli, A., Nicolai, E., Aiello, M., Tessa, C., Galli, L., Dotti, M.T., Piacentini, S., Salvatore, E., Toschi, N., 2014. Progression of brain atrophy in spinocerebellar ataxia type 2: a longitudinal tensor-based morphometry study. PLoS ONE 9 (2), e89410.
Mascalchi, M., Toschi, N., Giannelli, M., Ginestroni, A., Della Nave, R., Nicolai, E., Bianchi, A., Tessa, C., Salvatore, E., Aiello, M., Soricelli, A., Diciotti, S., 2015. Progression of microstructural damage in spinocerebellar ataxia type 2: a longitudinal DTI study. AJNR Am. J. Neuroradiol. 36 (6), 1096–10101.
Moriarty, A., Cook, A., Hunt, H., Adams, M.E., Cipolotti, L., Giunti, P., 2016. A longitudinal investigation into cognition and disease progression in spinocerebellar ataxia types 1, 2, 3, 6, and 7. Orphanet J. Rare Dis. 11 (1), 82.
O'Donnell, L.J., Westin, C.F., 2011. An introduction to diffusion tensor image analysis. Neurosurg. Clin. N. Am. 22 (2), 185–196.
Prakash, N., Hageman, N., Hua, X., Toga, A.W., Perlman, S.L., Salamon, N., 2009. Patterns of fractional anisotropy changes in white matter of cerebellar peduncles distinguish spinocerebellar ataxia-1 from multiple system atrophy and other ataxia syndromes. NeuroImage 47 (Suppl. 2), T72–T81.
Raffelt, D.A., Smith, R.E., Ridgway, G.R., Tournier, J.D., Vaughan, D.N., Rose, S., Henderson, R., Connelly, A., 2015. Connectivity-based fixel enhancement: whole-brain statistical analysis of diffusion MRI measures in the presence of crossing fibres. NeuroImage 117, 40–55.
Raffelt, D.A., Tournier, J.D., Smith, R.E., Vaughan, D.N., Jackson, G., Ridgway, G.R., Connelly, A., 2017. Investigating white matter fibre density and morphology using fixel-based analysis. NeuroImage 144 (Pt A), 58–73.
Reetz, K., Costa, A.S., Mirzazade, S., Lehmann, A., Juzek, A., Rakowicz, M., Boguslawska, R., Schöls, L., Linnemann, C., Mariotti, C., Grisoli, M., Dürr, A., van de Warrenburg, B.P., Timmann, D., Pandolfo, M., Bauer, P., Jacobi, H., Hauser, T.K., Klockgether, T., Schulz, J.B., 2013. Ataxia study group investigators. Genotype-specific patterns of atrophy progression are more sensitive than clinical decline in SCA1, SCA3 and SCA6. Brain 136 (Pt 3), 905–917.
Reuter, M., Rosas, H.D., Fischl, B., 2010. Highly accurate inverse consistent registration: a robust approach. NeuroImage 53 (4), 1181–1196.
Reuter, M., Schmansky, N.J., Rosas, H.D., Fischl, B., 2012. Within-subject template estimation for unbiased longitudinal image analysis. NeuroImage 61 (4), 1402–1418.
Rozenfeld, M.N., Nemeth, A.J., Walker, M.T., Mohan, P., Wang, X., Parrish, T.B., Opal, P., 2015. An investigation of diffusion imaging techniques in the evaluation of spinocerebellar ataxia and multisystem atrophy. J. Clin. Neurosci. 22 (1), 166–172.
Rüb, U., Schöls, L., Paulson, H., Auburger, G., Kermer, P., Jen, J.C., Seidel, K., Korf, H.W., Deller, T., 2013. Clinical features, neurogenetics and neuropathology of the polyglutamine spinocerebellar ataxias type 1, 2, 3, 6 and 7. Prog. Neurobiol. 104, 38–66.
Sawilowsky, S., 2009. New effect size rules of thumb. J. Mod. Appl. Stat. Methods 8 (2), 467–474.
Schlaier, J.R., Beer, A.L., Faltermeier, R., Fellner, C., Steib, K., Lange, M., Greenlee, M.W., Brawanski, A.T., Anthofer, J.M., 2017. Probabilistic vs. deterministic fiber tracking and the influence of different seed regions to delineate cerebellar-thalamic fibers in deep brain stimulation. Eur. J. Neurosci. 45 (12), 1623–1633.
Schmitz-Hübsch, T., du Montcel, S.T., Baliko, L., Berciano, J., Boesch, S., Depondt, C., Giunti, P., Globas, C., Infante, J., Kang, J.S., Kremer, B., Mariotti, C., Melegh, B., Pandolfo, M., Rakowicz, M., Ribai, P., Rola, R., Schöls, L., Szymanski, S., van de Warrenburg, B.P., Dürr, A., Klockgether, T., Fancellu, R., 2006. Scale for the assessment and rating of ataxia: development of a new clinical scale. Neurology 66 (11), 1717–1720.
Smith, S.M., Jenkinson, M., Johansen-Berg, H., Rueckert, D., Nichols, T.E., Mackay, C.E., Watkins, K.E., Ciccarelli, O., Cader, M.Z., Matthews, P.M., Behrens, T.E., 2006. Tract-based spatial statistics: voxelwise analysis of multi-subject diffusion data. NeuroImage 31 (4), 1487–1505.
Tabrizi, S.J., Scahill, R.I., Owen, G., Durr, A., Leavitt, B.R., Roos, R.A., Borowsky, B., Landwehrmeyer, B., Frost, C., Johnson, H., Craufurd, D., Reilmann, R., Stout, J.C., Langbehn, D.R., 2013. Predictors of phenotypic progression and disease onset in premanifest and early-stage Huntington's disease in the TRACK-HD study: analysis of 36-month observational data. Lancet Neurol. 12 (7), 637–649.
Vaughan, D.N., Raffelt, D., Curwood, E., Tsai, M.H., Tournier, J.D., Connelly, A., Jackson, G.D., 2017. Tract-specific atrophy in focal epilepsy: disease, genetics, or seizures? Ann. Neurol. 81 (2), 240–250.
Veraart, J., Novikov, D.S., Christiaens, D., Ades-Aron, B., Sijbers, J., Fieremans, E., 2016. Denoising of diffusion MRI using random matrix theory. NeuroImage 142, 394–406.
Wilkins, B., Lee, N., Gajawelli, N., Law, M., Leporé, N., 2015. Fiber estimation and tractography in diffusion MRI: development of simulated brain images and comparison of multi-fiber analysis methods at clinical b-values. NeuroImage 109, 341–356.
Wright, D.K., Johnston, L.A., Kershaw, J., Ordidge, R., O'Brien, T.J., Shultz, S.R., 2017. Changes in apparent fiber density and track-weighted imaging metrics in white matter following experimental traumatic brain injury. J. Neurotrauma 34 (13), 2109.
Yoo, Y.J., Oh, J., 2017. Identification of early neurodegenerative change in presymptomatic spinocerebellar ataxia type 1: a diffusion tensor imaging study. Parkinsonism Relat. Disord. 36, 109–110.
Yushkevich, P.A., Piven, J., Hazlett, H.C., Smith, R.G., Ho, S., Gee, J.C., Gerig, G., 2006. User-guided 3D active contour segmentation of anatomical structures: significantly improved efficiency and reliability. NeuroImage 31 (3), 1116–1128.